

Testing of global pressure/temperature (GPT) model and global mapping function (GMF) in GPS analyses

J. Kouba

Received: 19 December 2007 / Accepted: 3 April 2008
© Springer-Verlag 2008

Abstract Several sources of a priori meteorological data have been compared for their effects on geodetic results from GPS precise point positioning (PPP). The new global pressure and temperature model (GPT), available at the IERS Conventions web site, provides pressure values that have been used to compute a priori hydrostatic (dry) zenith path delay z_h estimates. Both the GPT-derived and a simple height-dependent a priori constant z_h performed well for low- and mid-latitude stations. However, due to the actual variations not accounted for by the seasonal GPT model pressure values or the a priori constant z_h , GPS height solution errors can sometimes exceed 10 mm, particularly in Polar Regions or with elevation cutoff angles less than 10 degrees. Such height errors are nearly perfectly correlated with local pressure variations so that for most stations they partly (and for solutions with 5-degree elevation angle cutoff almost fully) compensate for the atmospheric loading displacements. Consequently, unlike PPP solutions utilizing a numerical weather model (NWM) or locally measured pressure data for a priori z_h , the GPT-based PPP height repeatabilities are better for most stations before rather than after correcting for atmospheric loading. At 5 of the 11 studied stations, for which measured local meteorological data were available, the PPP height errors caused by a priori z_h interpolated from gridded Vienna Mapping Function-1 (VMF1) data (from a NWM) were less than 0.5 mm. Height errors due to the global mapping function (GMF) are even larger than those caused by the GPT a priori pressure errors. The GMF height errors are mainly due to the hydrostatic mapping and for the solutions with 10-degree elevation cutoff they are about 50% larger than the GPT a priori errors.

Keywords Troposphere mapping function · Tropospheric propagation delays · Meteorological data · Precise point positioning (PPP) · GPS · Atmospheric loading

1 Introduction

The Earth's atmosphere causes propagation delays of radio waves, typically exceeding 2 m at zenith. The propagation path delays consist of the hydrostatic (dry) and water vapor (wet) parts. The hydrostatic portion of the total zenith path delay (ZPD) can be accurately modeled from observed surface pressure and accounts for most of the atmospheric ZPD. The atmospheric water vapor is highly variable in most regions and is difficult to model, but typically causes 10% or more of the ZPD (e.g., Hopfield 1969). All radio space-geodetic techniques, such as very long baseline interferometry (VLBI) and global positioning system (GPS), are affected by both the predictable dry and the poorly known wet components of the atmosphere. Consequently, estimation of the wet portion of ZPD is a standard method in most high-accuracy geodetic applications. To prevent solution instability (singularity), only one ZPD unknown (wet ZPD) is introduced at any given epoch and station, either as a stochastic variable or random parameters valid over short intervals spanning several observation epochs.

Since observations are not generally made in the zenith direction, the ZPD has to be related (mapped) to the desired slant directions. This transformation of ZPD into the slant tropospheric delay is called a tropospheric mapping function (MF) and is normally performed separately for the dry and wet components due to their significantly different height distributions. Tropospheric mapping represents a major challenge since even the dominant hydrostatic part of the atmosphere is also highly variable, especially for low elevation

J. Kouba (✉)
Geodetic Survey Division, Natural Resources Canada (NRCAN),
615 Booth Street, Ottawa, Canada, K1A 0E9
e-mail: kouba@geod.nrcan.gc.ca

angle observations, which in turn are essential for the estimation of precise height and ZPD solutions.

Although the MF is roughly equal to $1/\sin E$, where E is the elevation angle, most precise analyses require a better formulation. Currently, the continued fractions in terms of $\sin E$, are most often used (see e.g., Marini 1972):

$$\text{mf}(E, a, b, c) = \frac{1 + \frac{a}{1 + \frac{b}{1+c}}}{\sin E + \frac{a}{\sin E + \frac{b}{\sin E+c}}}, \quad (1)$$

where the coefficients a , b and c are small ($\ll 1$) constants. Different sets of coefficients (a_h, b_h, c_h) and (a_w, b_w, c_w) are required for the hydrostatic and wet path delays, respectively. The required slant propagation delay (SPD) is then calculated:

$$\text{SPD}(E) = \text{mf}(E, a_h, b_h, c_h) \cdot z_h + \text{mf}(E, a_w, b_w, c_w) \cdot z_w, \quad (2)$$

where the hydrostatic zenith delay z_h is typically obtained from local surface meteorological measurements (Davis et al. 1985), a numerical weather model (NWM) (Schuh et al. 2006), or from a pressure and temperature model such as GPT (Boehm et al. 2007a; Tregoning and Herring 2006). The GPT model is a global spherical harmonic fit (degree and order nine) to three years of gridded monthly NWM pressure and temperature data to annual variations. So it accounts for major regional and seasonal scale variations only. In some analyses, only a very simple height-dependent pressure value has been assumed, independent of latitude and longitude (see e.g., Tregoning and Herring 2006, where the impact of the height-dependent pressure a priori z_h on height errors is studied).

The wet delay z_w is normally considered an unknown parameter and is estimated from observations. The hydrostatic delay z_h in Eq. 2 has to be known fairly accurately, since for low elevation angles the hydrostatic and wet MFs, $\text{mf}(E, a_h, b_h, c_h)$ and $\text{mf}(E, a_w, b_w, c_w)$, differ significantly. Consequently, any error in z_h cannot be fully absorbed into the estimated z_w , which then can cause position errors, mainly in height. Such errors are called hydrostatic/wet mapping separation errors. According to Boehm et al. (2006a), for 5-degree elevation cutoff, the hydrostatic/wet mapping separation causes height errors about one-tenth of the z_h error. Consequently, to achieve a 1 mm height accuracy, z_h has to be known a priori to within 1 cm when using data down to 5-degree elevation or within 2 cm for 10-degree elevation cutoff (see below). This stringent requirement normally requires either locally observed pressure values or the use of a NWM.

The main purpose of this paper is to evaluate the new global pressure and temperature model (GPT), recently developed by Boehm et al. (2007a) and to assess its accuracy and suitability for precise global GPS analyses. The GPT model

is available at the web sites of VMF1 (<http://mars.hg.tuwien.ac.at/~ecmwf1/>) and at the International Earth Rotation and Reference Systems Service (IERS) Conventions Product Center (http://tai.bipm.org/iers/conv2003/conv2003_c7.html). For GPT evaluation, precise point positioning (PPP) of a globally distributed subset of International GNSS Service (IGS) stations is used here to represent global GPS analyses. The validation of GPT was done with respect to the gridded VMF1 data, which itself was validated with the well-proven site-specific VMF1 data (Boehm and Schuh 2004; Boehm et al. 2006a) by Kouba (2007). The GPT validation was done in two steps. In the first step, z_h was computed from GPT model pressure and compared to the gridded VMF1 z_h , interpolated for specific time and site locations (see Kouba 2007), and the z_h differences were used to approximate their effect on height differences caused by the respective hydrostatic/wet mapping separations. For stations with measured meteorological data, the interpolated gridded VMF1 z_h was also compared to z_h obtained from the measured pressure and the differences were used to approximate the height errors caused by errors in the gridded VMF1 hydrostatic delays z_h . In the second step, NRCAN PPP solutions (Héroux and Kouba 2001) were compared for two approaches, using either the GPT model plus GMF global mapping functions (Boehm et al. 2006b) or gridded VMF1 values utilizing interpolated, time-dependent z_h delays together with time-dependent VMF1 MFs (i.e., the coefficients a_h and a_w). The PPP height differences include the effects of time-varying hydrostatic/wet mapping separation errors as well as the GMF/VMF1 MF differences.

For both steps, a globally distributed set of 11 IGS station data for the period of July 2004 to December 2005 was used. This set of 11 well-performing IGS stations (Table 1), representing the polar, mid-latitude and equatorial regions over a 1.5-year interval was considered to be a sufficient data

Table 1 Locations of the selected IGS stations used for GPT/GMF model testing with data from July 2004 to December 2005

IGS name	ϕ (degree)	λ (degree)	ell. h_s (m)
NYAL Ny-Alesund, Norway	78.93	11.87	82
YELL Yellowknife, Canada	62.48	245.52	181
WTZR Koetzing, Germany	49.14	12.88	666
ALGO Algonquin Park, Canada	45.96	281.93	202
TSK2 Tsukuba, Japan	36.11	140.09	70
KOKB Kokee Park, Waimea	22.13	200.34	1168
KOUR Kourou, French Guyana	5.25	307.19	-26
HARB Pretoria, South Africa	-25.89	27.71	1555
YAR2 Dongara, Australia	-29.05	115.35	241
OH12 O'Higgins, Antarctic P.	-63.32	302.10	33
MCM4 Ross Island, Antarctica	-77.84	166.67	98

sample for this purpose, i.e., a validation of the GPT/GMF models in global GPS analyses, represented here by PPP. PPP, utilizing IGS orbits/clocks combined solution products, facilitate efficient and convenient access to station position, wet ZPD and station clock solutions, which approximate global GPS solutions, since PPP can be viewed as a back substitution into the corresponding global GPS analyses. Unless stated otherwise, all the PPP solutions analyzed here used the IGS Final orbits/clocks, 10-degree elevation cutoff angle, an elevation data weighting proportional to $(\sin E)^2$, the gridded VMF1 (MF and z_h) with stochastic tropospheric gradient solutions (modeled as a random walk), and 15-min data sampling. From the above options, only the elevation cut-off and data weighting significantly effect the solution errors caused by errors of MF and a priori z_h . GPT model temperatures were not evaluated here, since z_h has almost no temperature dependence and can be approximated without temperature (see Eq. 3).

2 Hydrostatic/wet separation height errors

Consistent with Boehm et al. (2006a), the approximation of Davis et al. (1985) is used for z_h (in m):

$$z_h(h) = 0.0022768 \frac{p(h)}{(1 - 0.00266 \cos(2\varphi) - 0.28 \times 10^{-6}h)} \tag{3}$$

and that of Berg (1948) for the pressure lapse rate (in hPa):

$$p(h) = 1013.25(1 - 0.0000226h)^{5.225}, \tag{4}$$

where h is height (in meters). When the station pressure is available for latitude φ and height h , the hydrostatic delay $z_h(h)$ can be easily evaluated from Eq. 3. When the station pressure is taken at a different height, Eqs. 3 and 4 can be used to transfer the measured pressure and/or $z_h(h)$ to the station

height. Alternatively, for small height differences (<100 m), differentiating Eq. 4 yields an approximate pressure dependence on the station height of about -0.12 hPa/m. Substituting this into Eq. 3 then gives an approximate dependence of $z_h(h)$ (in mm) on height h (in m) of about -0.27 mm/m.

To evaluate the hydrostatic/wet mapping separation effects on PPP height solutions, the 11-station set was processed twice for 5 equally spaced days of 2005, in each case using a 10-degree elevation cutoff. The second processing was identical to the first except that z_h was increased by exactly 10 mm. The differences (in mm) for the PPP height solutions ($h(z_h + 10 \text{ mm}) - h(z_h)$) are shown in Table 2.

As seen in Table 2, the PPP height errors caused by a +10 mm error in z_h are equal to -0.5 mm, on average, and range from -0.4 mm at *algo* up to -0.7 mm at *nyal*. These height errors were evaluated for 10-degree elevation angle cutoff. For a 5-degree cutoff angle, the errors increase by a factor of about 2, as seen in Table 3, which shows the corresponding height changes for 5-degree elevation cutoff at the 6 of 11 stations with observational data down to 5 degrees. Table 3 results are consistent with Boehm et al. (2006a). The Antarctic stations (*mcm4* and *ohi2*) show larger apparent seasonal variations, with extrema during local summers and winters (see Tables 2 and 3). The high latitude station *nyal* has the greatest sensitivity to z_h errors for both 5- and 10-degree cutoffs, while *ohi2* is also distinctive for a 5-degree cutoff. Note that the Tables 2 and 3 results also depend on data weighting. For a weaker elevation dependent or identity (i.e., no elevation dependent) weighting, the hydrostatic/wet delay mapping separation errors are even larger than those in Tables 2 and 3. More specifically, when the analyses of Tables 2 and 3 were done with identity weighting (not shown here for brevity sake), the respective MF dry/wet separation changes in Tables 2 and 3 were increased by about 15 and 50% for 10- and 5-degree elevation cut-off, respectively.

Table 2 Hydrostatic/wet mapping separation height errors (mm) for +10 mm error in z_h and for 10-degree elevation cutoff PPP

Station	Latitude (degree)	1 January 2005	1 March 2007	1 July 2007	1 September 2007	1 January 2006	Mean
<i>nyal</i>	78.93	-0.7	-0.7	-0.7	-0.7	-0.7	-0.70
<i>yell</i>	62.48	-0.4	-0.5	-0.5	-0.6	-0.5	-0.50
<i>wtZR</i>	49.14	-0.4	-0.5	-0.5	-0.4	-0.4	-0.44
<i>algo</i>	45.96	-0.4	-0.4	-0.4	-0.4	-0.4	-0.40
<i>tsk2</i>	36.11	-0.6	-0.5	-0.5	-0.5	-0.5	-0.52
<i>kokb</i>	22.13	-0.5	-0.6	-0.5	-0.5	-0.5	-0.52
<i>kour</i>	5.25	-0.4	-0.3	-0.5	-0.4	-0.4	-0.40
<i>harb</i>	-25.89	-0.5	-0.5	-0.5	-0.5	-0.5	-0.50
<i>yar2</i>	-29.05	-0.5	-0.5	-0.5	-0.5	-0.5	-0.50
<i>ohi2</i>	-63.32	-0.6	-0.5	-0.4	-0.4	-0.5	-0.48
<i>mcm4</i>	-77.84	-0.7	-0.6	-0.5	-0.4	-0.6	-0.56
Mean		-0.52	-0.51	-0.50	-0.48	-0.50	-0.50

Table 3 Hydrostatic/wet mapping separation height errors (mm) for +10 mm error in z_h and for 5-degrees elevation cutoff PPP

Station	Latitude (degree)	1 January 2005	1 March 2007	1 July 2007	1 September 2007	1 January 2006	Mean
<i>nyal</i>	78.93	-1.4	-1.4	-1.3	-1.3	-1.2	-1.32
<i>wtzt</i>	49.14	-1.0	-1.1	-1.1	-1.1	-1.1	-1.08
<i>tsk2</i>	36.11	-1.1	-0.9	-0.9	-1.0	-1.1	-1.00
<i>kokb</i>	22.13	-0.9	-1.0	-0.9	-0.9	-1.1	-0.96
<i>ohi2</i>	-63.32	-1.1	-0.8	-0.8	-0.7	-0.7	-0.82
<i>mcm4</i>	-77.84	-1.2	-1.2	-0.8	-0.8	-1.1	-1.02
Mean		-1.12	-1.07	-0.97	-0.97	-1.05	-1.03

The regression coefficients of Table 2 were used to approximate the height errors caused by differences of z_h computed from GPT pressure (by Eqs. 3 and 4) and the z_h of the gridded VMF1 data. The results are plotted in Fig. 1. Here, one can see that due to significant non-seasonal pressure variations that are not included in the GPT model, the GPT height differences can reach up to about 6 mm (for *mcm4*). The overall RMS of the differences is 1.2 mm. All the stations, except for *mcm4* are unbiased and centered on zero. However, *mcm4* appears to have a small positive height bias of about 2 mm when using GPT instead of the gridded VMF1 z_h (see Fig. 1 and Table 4). This could signify a limitation of the GPT model (such as an inadequate resolution of the harmonic approximation) or gridded VMF1 data problems at *mcm4* (see below).

For completeness, also compiled were comparisons for a for z_h , based on a rather crude a priori pressure approximation sometimes used in GPS processing, which for each station assumes only a nominal, height-dependent z_h computed according to Eqs. (3) and (4). Though this simple approximation works surprisingly well for low- and mid-latitude stations, comparable to GPT, for high latitudes it causes

station height biases as well as small seasonal variations. The GPT model largely removed both the biases (compare Fig. 1 and Table 4, see also Boehm et al. 2007a; Tregoning and Herring 2006) as well as the small seasonal variations of the constant z_h . An interesting observation here is that both Antarctic stations (*ohi2* and *mcm4*) show similar, negative biases in Table 4, which may be an indication that a GPT model regional bias could be the source of the small positive bias for *mcm4* in Fig. 1 and Table 4. On the other hand, VMF1 data problems cannot be ruled out either, since when comparing the gridded and site-dependent VMF1 z_h , Kouba (2007) has also noticed biases and discontinuities up to 40 mm for *mcm4*.

3 PPP comparisons of the GPT/GMF and gridded VMF1 models

In the second step, PPP solutions with a priori z_h based on GPT pressures and GMF mappings were compared to solutions using gridded VMF1 data, for both the time-dependent MF coefficients as well as the time-dependent a priori z_h

Fig. 1 Approximation of the hydrostatic/wet mapping separation height differences with respect to gridded VMF1 PPP; caused by a priori z_h , derived from GPT model pressure varying only regionally and seasonally. The regression coefficients of Table 2 were used for the approximation

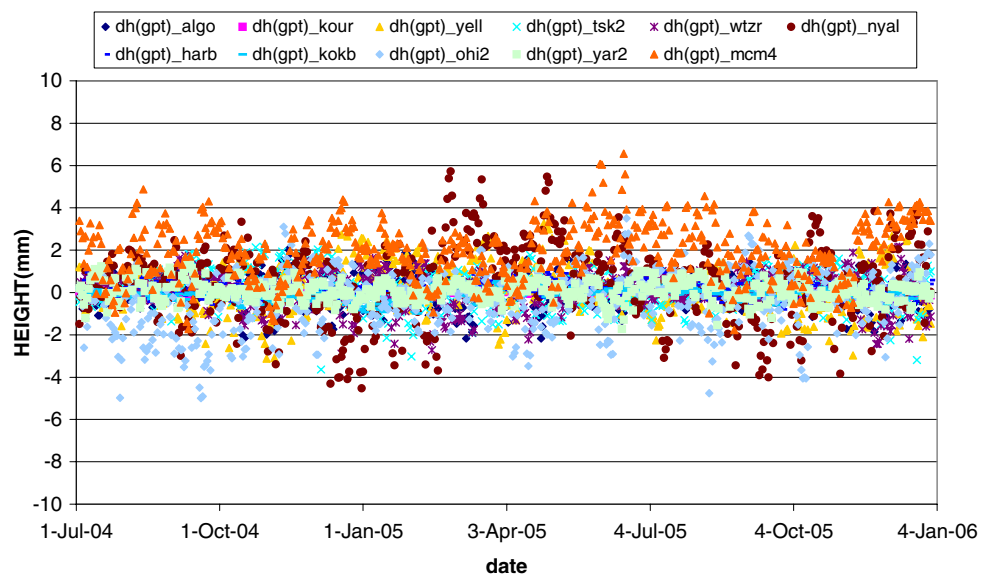


Table 4 Means and standard deviations (σ) of height differences with respect to gridded VMF1 PPP solutions; in the left half, listed are the differences of PPP solutions with **GMF/GPT** z_h , **GMF/ECMWF** z_h and with gridded VMF1 **MF/GPT** z_h

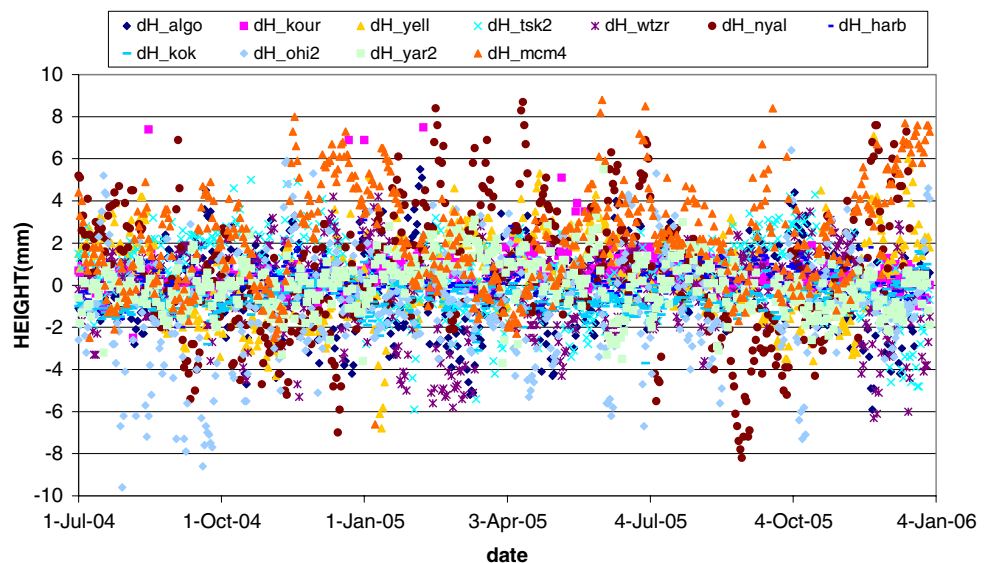
	GMF/GPT PPP		GMF PPP		GPT PPP		Constant z_h		GPT z_h		z_h (measured pressure)	
	Mean	σ	Mean	σ	Mean	σ	Mean	σ	Mean	σ	Mean	σ
<i>nyal</i>	0.6	3.1	0.3	2.5	0.3	1.7	-1.0	1.9	0.4	1.8		
<i>yell</i>	0.4	2.0	0.2	2.0	0.2	1.1	-0.8	1.1	0.2	1.1	0.1	0.1
<i>wtzt</i>	-0.4	2.0	-0.5	1.5	0.1	0.9	0.9	0.8	0.1	0.8	-0.1	0.1
<i>algo</i>	-0.1	2.0	-0.2	1.7	0.1	0.8	-0.5	0.9	0.1	0.9	-0.2	0.2
<i>tsk2</i>	0.5	1.8	0.3	1.5	0.1	0.8	0.5	0.8	0.2	0.8		
<i>kokb</i>	-0.7	0.6	-0.7	0.5	0.0	0.3	0.5	0.3	-0.1	0.3	-0.4	0.1
<i>kour</i>	0.5	0.9	0.5	0.8	0.0	0.4	-0.6	0.2	0.0	0.2		
<i>harb</i>	0.2	0.7	-0.1	0.7	0.3	0.5	1.3	0.4	0.2	0.3		
<i>yar2</i>	0.0	1.2	0.0	1.2	0.0	0.6	0.2	0.6	0.1	0.5		
<i>ohi2</i>	-0.9	2.6	-0.3	1.7	-0.6	1.4	-3.0	1.4	-0.4	1.4	-0.4	0.2
<i>mcm4</i>	2.3	2.6	0.7	1.8	1.6	1.2	-5.3	1.6	2.1	1.5		
Mean	0.2	1.8	0.0	1.4	0.2	0.9	-0.7	0.9	0.3	0.9	-0.2	0.1
σ	0.9	0.8	0.4	0.6	0.5	0.4	1.9	0.6	0.7	0.5	0.2	0.0

Also shown (in the right half of the table) are the height difference approximations, based on $-0.05 dz_h$ for dz_h differences, derived from height-dependent **constant** z_h , **GPT** z_h and **measured pressure** z_h , with respect to the ECMWF z_h ; units - mm

delays. The gridded VMF1 data is derived from a 2.0 by 2.5-degree latitude/longitude grid of the NWM of the European Centre for Medium-Range Weather Forecasts (ECMWF) at 6-h intervals. For each epoch, the gridded data set includes the MF coefficients (a_h, a_w) and the hydrostatic and wet zenith delays (z_h, z_w). Gridded VMF1 values were compared and validated with respect to the already well-established site-dependent VMF1 (Boehm and Schuh 2004; Boehm et al. 2006a) by Kouba (2007). However, unlike the site-dependent VMF1 time series, the gridded VMF1 model is available globally for all epochs since 1994.

The height differences (GPT/GMF PPP – gridded VMF1 PPP) for all the 11 GPS stations are plotted in Fig. 2. This time, in addition to mapping separation height differences (Fig. 1), the height differences of Fig. 2 also include the differences between GMF and the gridded VMF1 MF (both hydrostatic and wet parts). The height differences vary considerably and approach 10 mm for three of the four highest latitude stations. The corresponding differences for the horizontal components (not shown here) are virtually zero, except for a few 1–2 mm differences at the polar stations. A closer inspection has revealed that most of these small horizontal

Fig. 2 GPT/GMF PPP height differences with respect to the gridded VMF1 PPP; (GPT/GMF PPP – gridded VMF1 PPP) for 10-degree elevation angle data cutoff. (Includes differences in MFs and hydrostatic/wet mapping separations)



differences were caused by different data editing, rather than by the GPT and MF differences.

When comparing Figs. 1 and 2 it is apparent that, except for the equatorial stations where pressure variations are small, a significant part of the height differences in Fig. 2 is due to the hydrostatic/wet mapping separation errors shown in Fig. 1, particularly for the high-latitude stations. To demonstrate this, the PPP height differences of Fig. 2 and the approximation of the mapping separation errors of Fig. 1 are compared for the polar station *nyal* in Fig. 3. One can see here that at this station, the hydrostatic/wet mapping separation differences are indeed the major source of the GPT/GMF-gridded VMF1 PPP height differences and the biases seen in Fig. 2. Conversely, Figs. 2–3 confirm that the simple regression approximations of the height errors, caused by the hydrostatic/wet mapping separation differences shown in Fig. 1, are reasonable.

Figures 1–3 raise the question of the accuracy of the interpolated gridded VMF1 z_h (here after referred as ECMWF z_h). The comparisons of the ECMWF z_h (based on the $2.0 \times$

2.5-degree ECMWF NWM) and the site -VMF1 z_h data (based on the 0.25×0.25 degree ECMWF NWM) yielded an agreement at the 3-mm RMS level, except for *mcm4* and *harb*, where biases and discontinuities were up to 40 mm (Kouba 2007). Nevertheless, such comparisons are not independent and may not indicate the actual accuracy or robustness of the NWM derived z_h , since only different versions of the same agency NWM were used. To verify the accuracy of the ECMWF z_h for stations with measured barometric pressures, the ECMWF z_h were also compared to the z_h , computed from the locally measured pressure using Eqs. 3 and 4. Only four stations (*kokb*, *ohi2*, *wzr* and *yell*) of the 11 station set have measured meteorological data available from IGS. Additionally, *algo* meteorological data files were obtained directly from NRCan. For these five stations the hydrostatic/wet mapping separation height differences were also approximated by $-0.05 \times (z_h(\text{measured } p) - \text{ECMWF } z_h)$. These differences in fact approximate the height errors caused by the ECMWF z_h errors, since the measured pressure accuracy and biases are likely well below 1 hPa, which

Fig. 3 *nyal* GPT/GMF-gridded VMF1 PPP height differences (dH) and the hydrostatic/wet mapping separation errors for GPT z_h (approximated by $dh(gpt) = -0.07dz_h$) with respect to ECMWF z_h

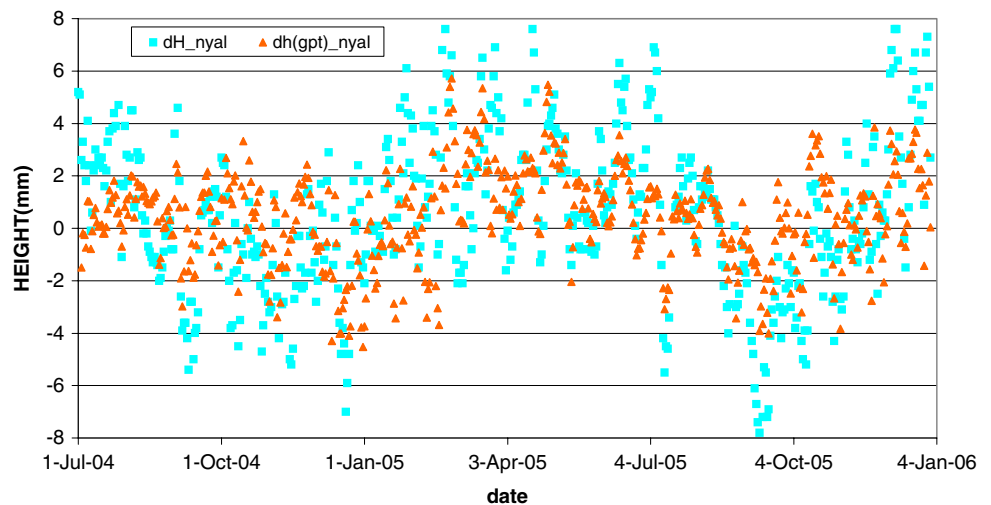
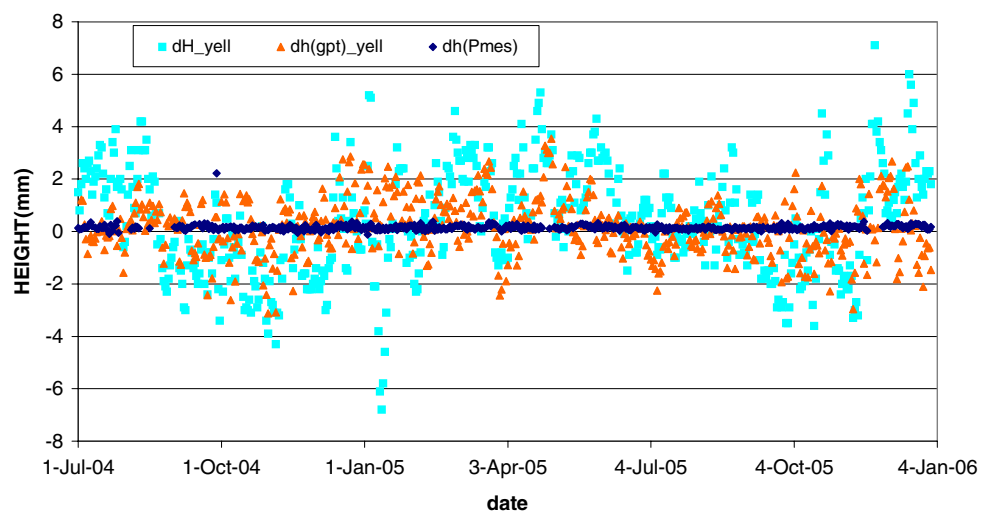


Fig. 4 *yell* height differences for GPT/GMF PPP solutions with respect to the gridded VMF1 PPP (dH) and approximations of hydrostatic/wet mapping separation height differences, obtained from GPT z_h ($dh(gpt)$) and from the measured pressure z_h ($dh(Pmes)$), respectively



corresponds to mapping separation height bias/errors of less than 0.1 mm.

Figure 4 shows three different types of height differences for station *yell*, all with respect to the “reference” PPP, obtained with the gridded VMF1 MF and ECMWF z_h . Namely, the differences of PPP with GMF/GPT and the two approximations of the hydrostatic/wet mapping separation height differences, derived from z_h , based on GPT pressure and the measured station pressure. The other four stations had similar agreement, thus are not shown here. As one can see in Fig. 4, the height agreement of the ECMWF and the measured pressure z_h is indeed impressive. The height biases are below 0.5 mm and the RMS agreement varied from 0.1 to 0.2 mm (see Table 4), which correspond to ECMWF z_h biases below 10 mm (or equivalently, 5 hPa for ECMWF pressure) and RMS agreement between 2 to 4 mm (or 1 and 2 hPa). Such an accuracy (of the ECMWF z_h) is quite sufficient to control the mapping separation errors at the sub mm level. However, there are some larger differences and gaps for the measured pressure height differences. Most of them are after gaps, so they likely pertain to pressure instrumentation problems. Note that in order to reduce over-sampling and to facilitate a direct comparison with PPP, only one epoch (0-h UT) was used for the GPT and measured pressure height differences. Ideally, since pressure variation is positively auto-correlated over several days (Boehm and Schuh 2007b), even longer sampling intervals could have been used in order to obtain more meaningful statistics listed in Table 4.

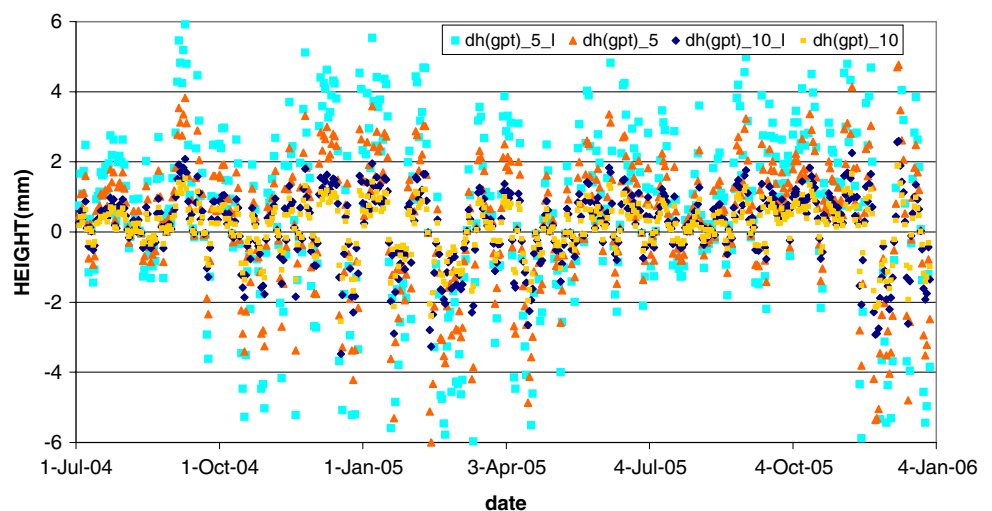
Figure 5 compares the approximations of hydrostatic/wet mapping separation height differences at station *wtzr* for 10- and 5-degree elevation cutoffs, and identity data weighting. Here one can observe that the height differences for 5-degree elevation cutoff and with identity weighting are larger than the height differences with 10-degree cutoff and elevation dependent data weighting by a factor up to 3. Boehm et al. (2006c) investigated also the height differences of

hydrostatic and wet GMF MF with respect to VMF1 MF for 5-degree elevation cutoff. The hydrostatic GMF MF height differences (errors) were larger by about 30% than the hydrostatic/wet mapping separation differences, with a similar behavior; i.e., they were largest in high latitudes and smallest in equatorial regions. The wet GMF height differences were smaller and had the opposite behavior; i.e., they were smallest in high latitudes and largest near the equator, where they were of similar magnitude to the mapping separation height differences (Boehm et al. 2006c). For 10-degree elevation cutoff, the height GMF differences are also larger than the mapping separation height errors as seen in Table 4, which shows statistics of PPP height solutions differences with respect to gridded VMF1, caused by GMF/GPT, GMF MF and GPT model. Here one can see that for most stations the GMF PPP height solution differences (col. 4–5) are about 50% larger than the GPT PPP ones (col. 6–7). Furthermore, the GPT height difference approximations (in col. 10–11), based on regression coefficients of Table 2, also agree quite well with the actual GPT PPP differences (col. 6–7). For completeness, statistics for the approximations with the constant and measured pressure z_h are also listed here.

4 Discussions

The hydrostatic/wet mapping separation height errors appear random in Fig. 1, however, they are far from random and in fact they are rather systematic and perfectly correlated with atmospheric pressure, since they were derived from the local pressure variation. Much like the pressure, they are positively autocorrelated and thus can be forecast for up to 5 days (Boehm and Schuh 2007b). Furthermore, they are also correlated over broad regions of several hundred of km, so they will not show up in height solution repeatability over short time intervals or in regional differential height solutions.

Fig. 5 Approximations of *wtzr* hydrostatic/wet mapping separation height differences of GPT z_h with respect to ECMWF z_h ; for 5- and 10-degree elevation data cutoff with the elevation angle weighting ($dh(gpt)_5$; $dh(gpt)_10$) and with the identity weighting ($dh(gpt)_5_I$; $dh(gpt)_10_I$). The mean regression coefficients of -0.16 , -0.11 , -0.06 and -0.05 were used for $dh(gpt)_5_I$; $dh(gpt)_5$, $dh(gpt)_10_I$ and $dh(gpt)_10$, respectively



These facts make the hydrostatic/wet mapping separation errors even more dangerous, since they can diminish various applications, which rely on atmospheric pressure, such as various loading or gravity change analyses (e.g. see [Blewitt et al. 2001](#)). This is also demonstrated by Table 5, which lists the atmospheric loading (AL) regression coefficients and their formal solution errors, evaluated by linear regressions of daily PPP height solutions and NWM pressure variations (computed from ECMWF z_h , using Eqs. (3) and (4)) over the 1.5-year interval. For comparisons, the AL regression coefficients of the IERS 2003 Conventions (see <http://tai.bipm.org/iers/conv2003/chapter7/atmospheric.regr>) are also listed here. Since AL derived from position solutions were considered unreliable (see IERS 2003 Convention, Chap. 7), the IERS regression coefficients have been derived from a geophysical model and pressure data from the 18 years of the U.S. National Center for Environment Prediction (NCEP) Reanalysis during 1980–1998. For completeness, Table 5 also shows the correlation coefficients of the gridded VMF1 PPP height solutions with respect to the ECMWF pressures. The correlation coefficients of Table 5 are consistent but small (and for GMF/GPT PPP they are even smaller than for the gridded VMF1 PPP); this is likely due to other significant height errors, not correlated with pressure. From the differences in Table 5, one can see that the GPT/GMF PPP values are positively biased by as much as +0.2 mm/hPa, relative to the gridded VMF1 PPP coefficients, which can represent up to 50% of the AL deformation signal. This destructive interference of GPT pressure errors and AL has already been noticed by [Tregoning and Herring \(2006\)](#). Depending on the elevation weighting and/or elevation angle cutoff, the

GPT errors and the apparent AL biases can be larger by a factor of 3, thus even exceeding 100% of the AL displacements. Note the unrealistic AL solutions for station *kour*, which is caused by a nearly constant ECMWF pressure for that station and this is also reflected by the largest formal solution error of about 0.4 mm/hPa. Consequently, the *kour* AL regression determination is rather uncertain and likely overwhelmed with other (PPP solution) height errors and the *kour* values are excluded from the Table 5 means.

In fact, the GPT mapping separation height errors (Fig. 1) partly compensate for the atmospheric effects, making GPT PPP height repeatabilities better than for gridded VMF1 PPP heights before correcting for the AL effects. This is demonstrated by Table 6, which lists daily height solution repeatability for GPT/GMF and gridded VMF1 PPP, before and after correcting for the IERS03 AL regression coefficients of Table 5. In most cases, the uncorrected gridded VMF1 PPP repeatability is worse (due to the AL effects) than for uncorrected GPT/GMF PPP, while the repeatability of the gridded VMF1 PPP height solutions, corrected for AL, in most cases becomes better than the corresponding GPT/GMF PPP solution repeatability. Even though the average improvement of the gridded VMF1 height repeatability of 9.88 mm over the GPT/GMF one of 10.00 mm in Table 6 seems to be rather small and insignificant, one should realize that this difference is equivalent to a systematic (pressure correlated) signal with σ of 1.5 mm. Furthermore, for 5-degree elevation angle cutoff or identity data weighting the relative AL improvements seen in Table 6 will be even more pronounced and significant, by up to a factor of 3.

Table 5 Height atmospheric loading regression coefficients (a_{AL}) and their formal solution errors (1σ) in mm/hPa, derived by linear regressions of daily gridded VMF1 or GPT/GMF PPP height solutions and the ECMWF pressure, during July 2004–December 2005

Name	IERS03	Gridded VMF1			GMF/GPT			GMF/GPT-gridded VMF1		
	a_{AL}	a_{AL}	σ	ρ	a_{AL}	σ	ρ	da_{AL}	σ	$d\rho$
<i>nyal</i>	−0.20	−0.11	0.03	−0.19	0.04	0.03	0.06	0.15	0.04	0.25
<i>yell</i>	−0.46	−0.37	0.04	−0.47	−0.29	0.04	−0.39	0.08	0.06	0.08
<i>wtzt</i>	−0.44	−0.42	0.05	−0.39	−0.23	0.04	−0.20	0.19	0.06	0.19
<i>algo</i>	−0.30	−0.27	0.04	−0.34	−0.14	0.04	−0.18	0.13	0.06	0.16
<i>tsk2</i>	−0.13	−0.25	0.06	−0.21	−0.10	0.06	−0.09	0.15	0.08	0.12
<i>kokb</i>	−0.18	−0.46	0.18	−0.10	−0.36	0.19	−0.08	0.10	0.26	0.02
<i>kour</i> ^a	−0.46	−2.44	0.38	−0.29	−2.33	0.38	−0.28	0.11	0.54	0.01
<i>harb</i>	−0.57	−0.21	0.10	−0.10	−0.24	0.10	−0.11	−0.03	0.14	−0.01
<i>yar2</i>	−0.42	−0.79	0.08	−0.42	−0.78	0.09	−0.41	0.01	0.12	0.01
<i>ohi2</i>	−0.23	−0.10	0.07	−0.10	0.05	0.07	0.02	0.15	0.10	0.12
<i>mcm4</i>	−0.49	−0.50	0.06	−0.39	−0.31	0.06	−0.25	0.19	0.08	0.14
Mean	−0.35	−0.35	0.07	−0.27	−0.24	0.07	−0.16	0.11	0.10	0.11

Also shown are the atmospheric loading coefficients from the IERS2003 Convention web site and the correlation coefficients (ρ) of the PPP height solutions with the VMF1 NWM pressure. The last columns list statistics for corresponding differences

^a Excluded from the means (see the text)

Table 6 Daily PPP height solution repeatabilities (in mm) with the elevation angle weighting and 10-degree elevation cutoff, before (σ_h) and after (σ_{h_al}) correcting with the IERS03 AL regression coefficients (see Table 5), during July 2004–December, 2005

Station	GPT/GMF PPP		Grid VMF1 PPP	
	σ_h	σ_{h_al}	σ_h	σ_{h_al}
<i>nyal</i>	6.8	7.3	7.2	7.2
<i>yell</i>	7.5	7.1	7.8	7.0
<i>algo</i>	6.8	6.8	6.7	6.4
<i>wtzt</i>	7.2	7.2	7.6	7.1
<i>tsk2</i>	8.6	8.5	9.0	8.8
<i>kokb</i>	9.8	9.7	9.7	9.7
<i>kour</i>	12.7	12.5	12.7	12.6
<i>harb</i>	7.5	7.5	7.7	7.7
<i>yar2</i>	9.3	8.7	9.1	8.5
<i>ohi2</i>	16.0	16.2	16.1	16.0
<i>mcm4</i>	13.6	13.3	13.9	12.9
RMS	10.06	10.00	10.20	9.88

The main purpose of Table 6 was to explain this surprising paradox. Namely that, unless the height solutions, based on measured or NWM pressure are corrected for AL, they may appear to have a worse repeatability than the corresponding uncorrected height solutions with hydrostatic delays z_h , derived from height dependent constant or GPT model pressure. Thus, the above AL analyses and its applications to height solutions are empirical and approximate only. Nevertheless, they are considered adequate for the purpose, i.e., to show that for most stations the mapping separation errors are correlated with AL height displacements. Furthermore, according to (http://tai.bipm.org/iers/conv2003/conv2003_c7.htm), such AL regression coefficients, determined from precise and unbiased geodetic height solutions may be potentially more precise than those determined from globally convoluted geophysical models, currently recommended by the IERS 2003 Conventions.

The PPP should represent well the effects of GPT/GMF errors on station solutions (positions, ZPD and station clocks) of global GPS analyses. Namely, the station clock solutions like for PPP, also fully reflect the height errors of Fig. 1, while the corresponding ZPD are about 30% (Gendt 1998) of the height errors of Fig. 1. On the other hand, PPP solutions cannot be used to assess the GPT/GMF model effects on the solutions of earth rotation parameters (ERP) as well as the satellite parameters (orbits and satellite clocks), since these are fixed in PPP. However, since the GPT/GMF model errors have virtually no effect on station horizontal solutions, ERP solutions also should not be significantly affected for well distributed and sufficiently dense station networks (such as those used in IGS global analyses). The corresponding satellite

parameter solutions (clock and orbits) will be affected, but to a smaller extent than the station parameter solutions due to averaging over several stations, simultaneously observing a satellite and since in global analyses such stations will likely cover areas larger than the pressure systems. The orbit solutions errors will be even further mitigated thanks to the orbit dynamics. So, the satellite clock and the orbital errors in particular, should be smaller than those shown in Fig. 1 and they likely are negligible. However, the above presumptions need to be verified within global GPS analyses, using real data.

5 Conclusions

The GPT pressure model removes most height solution biases (Table 4) and the seasonal variations seen for constant, height-dependent a priori hydrostatic zenith delays z_h as already concluded by Tregoning and Herring (2006). However, the non-seasonal pressure variations, not accounted for in GPT, are even larger than the modeled regional and seasonal biases. In particular in high-latitude regions, they can cause pressure correlated height errors up to 10 mm, or even larger for 5-degree elevation angle cutoff or when identity data weighting is used. This is due to erroneous hydrostatic/wet mapping separations, which causes height errors up to 20% of the error in the hydrostatic zenith delays z_h . This means that for a sub-mm height accuracy, sub-cm accuracy of z_h is required, which in turn means that pressure must be known better than the 5 hPa accuracy level. Such pressure accuracy can be obtained only from local measurements, or alternatively from a state-of-art NWM, such as the one used for generations of the VMF1 data.

The ECMWF z_h data was also found to be sufficiently accurate for sub-mm height solutions. The mean height errors caused by the ECMWF z_h were 0.5 mm or less, with σ of 0.1–0.2 mm, as seen from the comparisons with measured pressure at the five of the 11 test stations, for which the measured pressure files were available (Table 4; Fig. 4). This comparison of ECMWF z_h with z_h computed from measured pressure then implies ECMWF pressure biases of less than 5 hPa with RMS of 1–2 hPa. This level of agreement is comparable to the internal comparisons between the gridded and site VMF1 data in Kouba (2007).

Since VMF1 was shown to provide the most accurate VLBI solutions (Boehm et al. 2006a) and because thanks to the gridded VMF1, VMF1 data (VMF1 MF, including z_h) are now readily available anywhere and anytime after 1994, it is important that VMF1 data is used for the most precise geodetic solutions. GMF related height errors are even larger than the GPT ones for 5-degree and also for 10-degree elevation cutoff, so the time-varying VMF1 MF coefficients should also be used, along with the ECMWF z_h of VMF1 data set. For example, all the IGS global processing and the

reprocessing in particular, should make the use of VMF1 data mandatory, since a major motivation for any IGS reprocessing endeavor has to be the use of the best available data and models. The GMF/GPT were shown to be inadequate for this purpose, since they are causing pressure correlated height errors up to 10 mm and even more for elevation cutoff angles less than 10 degrees and/or for the identity data weighting. Even a more precise and optimal alternative than a NWM z_h would be to use locally measured pressure data, however, the lack of availability and reliability makes this optimal solution rather uncertain, or even impractical.

Acknowledgments The IGS data and combined solution products (Dow et al. 2005) were used here. The gridded VMF1 data as well as the *VMF1*, *GMF* and *GPT* subroutines are conveniently made available by The Institute of Geodesy and Geophysics, Vienna University of Technology (VUT), Vienna, Austria. Jim Ray of NGS/NOAA, Johannes Boehm of VUT, Peter Steigenberger of Geoforschungszentrum Potsdam and Paul Tregoning of the Australian National University, Canberra, have reviewed this paper and provided numerous suggestions and comments.

References

- Berg H (1948) Allgemeine meteorologie. Dümmlers, Bonn
- Blewitt G, Lavallée D, Clarke P, Nurutdinov K (2001) A new global mode of earth deformation: seasonal cycle detected. *Science* 294: 2342–2345
- Boehm J, Schuh H (2004) Vienna mapping functions in VLBI analyses. *Geophys Res Lett* 31:L01603. doi:[10.1029/2003GL018984](https://doi.org/10.1029/2003GL018984)
- Boehm J, Werl B, Schuh H (2006a) Troposphere mapping functions for GPS and very long baseline interferometry from European Centre for Medium-Range Weather Forecasts operational analysis data. *J Geophys Res* 111:B02406. doi:[10.1029/2005JB003629](https://doi.org/10.1029/2005JB003629)
- Boehm J, Niell A, Tregoning P, Schuh H (2006b) Global mapping function (GMF): a new empirical mapping function based on numerical weather model data. *Geophys Res Lett* 33:L07304. doi:[10.1029/2005GL025546](https://doi.org/10.1029/2005GL025546)
- Boehm J, Heinkelmann R, Schuh H (2006c) Neutral atmosphere delays: empirical models versus discrete time series from numerical weather models. In: Proceedings of IAG Symposium Geodetic Reference Frame (GRF2006), Munich, Germany, 9–13 October 2006 (in press)
- Boehm J, Heinkelmann R, Schuh H (2007a) Short note: a global model of pressure and temperature for geodetic applications. *J Geod* doi:[10.1007/s00190-007-0135-3](https://doi.org/10.1007/s00190-007-0135-3)
- Boehm J, Schuh H (2007b) Forecasting data of the troposphere used for IVS Intensive sessions. In: Boehm J, Pany A, Schuh H (eds) Proceedings of the 18th European VLBI for Geodesy and Astrometry Working Meeting, 12–13 April. Geowissenschaftliche Mitteilungen, Heft Nr. 79, Schriftenreihe der Studienrichtung Vermessung und Geoinformation. Technische Universität Wien, ISSN 1811–8380, pp 153–157
- Davis JL, Herring TA, Shapiro II, Rogers AEE, Elgered G (1985) Geodesy by radio interferometry: effects of atmospheric modeling errors on estimates of baseline length. *Radio Sci* 20(6): 1593–1607
- Dow JM, Neilan RE, Gendt G (2005) The International GPS Service (IGS): celebrating the 10th anniversary and looking to the next decade. *Adv Space Res* 36(3):320–326. doi:[10.1016/j.asr.2005.05.125](https://doi.org/10.1016/j.asr.2005.05.125)
- Gendt G (1998) IGS combination of tropospheric estimates—experience from pilot experiment. In: Dow JM, Kouba J, Springer T (eds) Proceedings of 1998 IGS Analysis Center Workshop. IGS Central Bureau, Jet Propulsion Laboratory, Pasadena, pp. 205–216
- Héroux P, Kouba J (2001) GPS precise point positioning with IGS orbit products. *Phys. Chem. Earth A* 26: 573–578
- Hopfield HS (1969) Two-quadratic tropospheric refractivity profile for correcting satellite data. *J Geophys Res* 74: 4487–4499
- Kouba J (2007) Implementation and testing of the gridded Vienna mapping function 1 (VMF1). *J Geod* doi:[10.1007/s00190-007-0170-3](https://doi.org/10.1007/s00190-007-0170-3)
- Marini JW (1972) Correction of satellite tracking data for an arbitrary tropospheric profile. *Radio Sci* 7(2): 223–231
- Schuh H, Panafidina N, Boehm J, Heinkelmann R (2006) Climatic signals observed by VLBI. *Acta Geod Geophys Hung* 41(2):159–170. doi:[10.1556/AGeod.41.2006.2.1](https://doi.org/10.1556/AGeod.41.2006.2.1)
- Tregoning P, Herring TA (2006) Impact of a priori zenith hydrostatic delay errors on GPS estimates of station heights and zenith total delays. *Geophys Res Lett* 33:L23303. doi:[10.1029/2006GL027706](https://doi.org/10.1029/2006GL027706)